Chinese Chemical Letters 37 (2026) 111981

Contents lists available at ScienceDirect

Chinese Chemical Letters

journal homepage: www.elsevier.com/locate/cclet

Glucose/ROS dual-responsive hydrogel loaded with mangiferin accelerates diabetic wound healing

Lele Meng[a,b,1], Ruhe Zhang[c,1], Liying Wang[d,*], Yuanzheng Wang[a], Bo Li[a], Long Chen[a,b,*]

[a] Department of Orthopedics, Guizhou Provincial People's Hospital, Guiyang 550000, China
[b] College of Orthopedics and Traumatology, Guizhou University of Traditional Chinese Medicine, Guiyang 550025, China
[c] Department of Hematology, The Seventh Affiliated Hospital, Sun Yat-sen University, Shenzhen 518107, China
[d] Department of Anesthesiology, General Hospital of Southern Theatre Command of PLA, Guangzhou 510010, China

ARTICLE INFO

Article history:
Received 5 August 2025
Revised 14 October 2025
Accepted 16 October 2025
Available online 17 October 2025

Keywords:
Diabetic wounds
Hydrogel
Mangiferin
Antioxidation
Anti-inflammatory

ABSTRACT

Diabetic wounds are characterized by local oxidative stress, bacterial infection, and persistent inflammation, all of which hinder effective clinical healing. To address these challenges, we developed a glucose/reactive oxygen species (ROS) dual-responsive hydrogel (hyaluronic acid-phenylboronic acid (HA-PBA)/polyvinyl alcohol (PVA)/mangiferin (MF), HPM) composed of HA-PBA and PVA. This hydrogel incorporates MF, a bioactive compound with multiple therapeutic properties, through dynamic boronate ester bonds, enabling stimulus-responsive drug release tailored to the diabetic wound microenvironment, thereby enhancing wound repair. Physicochemical analyses demonstrated that HPM exhibits a favorable porous structure, excellent swelling behavior, appropriate rheological characteristics, and self-healing capability. *In vitro* studies revealed that HPM effectively scavenges ROS, inhibits bacterial proliferation, attenuates inflammation, and promotes angiogenesis. In a diabetic rat model, HPM significantly accelerated wound closure, as indicated by enhanced epithelial regeneration, increased collagen deposition, improved neovascularization, and suppressed inflammatory. Moreover, biocompatibility evaluations confirmed the excellent biosafety of HPM both *in vitro* and *in vivo*. This multifunctional hydrogel dressing, combining glucose and ROS sensitivity with robust therapeutic efficacy and biocompatibility, offers a promising strategy for diabetic wound management.

© 2026 Published by Elsevier B.V. on behalf of Chinese Chemical Society and Institute of Materia Medica, Chinese Academy of Medical Sciences.

The impaired healing of diabetic wounds is driven by a multifactorial interplay involving hyperglycemia, oxidative stress, chronic inflammation, vascular and neural complications, and bacterial infection [1,2]. Under physiological conditions, wound healing progresses through the dynamically interconnected phases of hemostasis, inflammation, proliferation, and remodeling. In diabetes, however, persistent hyperglycemia induces excessive production of reactive oxygen species (ROS) and disrupts antioxidant defenses, leading to cellular damage and impaired M1/M2 macrophage polarization. This disturbance prolongs the inflammatory phase and hinders subsequent healing [3,4]. Moreover, hyperglycemia facilitates bacterial proliferation and biofilm formation, which further aggravate inflammation and compromise angiogenesis, thereby perpetuating a vicious cycle [5,6]. This complex pathological cascade progressively deteriorates the wound microenvironment and may culminate in severe infections [7]. Consequently, therapeutic strategies targeting ROS elimination, inflammation modulation, infection control, and the promotion of angiogenesis and tissue regeneration are essential for improving diabetic wound healing [8,9].

In recent years, various advanced wound dressings have been developed to address the persistent challenge of diabetic wound healing [10]. Among these, hydrogel dressings have garnered significant attention due to their excellent biocompatibility, moisture retention, and drug-loading capacity [11]. Hydrogels derived from natural polymers such as hyaluronic acid (HA) and sodium alginate exhibit distinct advantages; notably, HA has emerged as an ideal matrix material owing to its superior hydration properties, pro-angiogenic activity, and immunomodulatory effects [12]. Currently, multifunctional hydrogels incorporating antioxidant, antibacterial, and anti-inflammatory functionalities have been engineered to effectively regulate the wound microenvironment [13]. Nevertheless, traditional dressings remain limited by poor conformity to irregular wound surfaces and a lack of responsiveness to environmental stimuli [14]. Consequently, smart hydrogels capable of respond-

* Corresponding authors.
E-mail addresses: wangly53@mail2.sysu.edu.cn (L. Wang), longchen@gzu.edu.cn (L. Chen).
[1] These authors contribute equally to this work.

https://doi.org/10.1016/j.cclet.2025.111981
1001-8417/© 2026 Published by Elsevier B.V. on behalf of Chinese Chemical Society and Institute of Materia Medica, Chinese Academy of Medical Sciences.

ing to glucose, ROS, and pH fluctuations have received increasing interest. Additionally, composite hydrogels that integrate multiple bioactive components, such as natural therapeutic agents, are being developed to achieve synergistic effects across various therapeutic targets, including antimicrobial, anti-inflammatory, antioxidant, and angiogenic responses [15].

Mangiferin (MF) is a natural polyphenolic compound classified as a *C*-glucosyl xanthone, extracted from various plant families including Gentianaceae, Zingiberaceae, and Anacardiaceae, and is abundantly present in mangoes and papayas [16,17]. Due to its wide range of biological activities, such as hypoglycemic, antioxidant, anti-inflammatory, antibacterial, antiviral, anti-apoptotic, and pro-angiogenic effects, MF has garnered significant scientific interest. Recent research indicates that MF modulates numerous biological pathways involved in carbohydrate and lipid metabolism, thereby ameliorating metabolic dysfunctions and related diseases in both animal models and humans. These attributes underscore its potential in the prevention and treatment of diabetic wounds [18–20]. Moreover, MF exhibits anti-aging properties by mitigating the production of ROS induced by external stressors such as ultraviolet radiation, and by inhibiting the enzymatic activity of skin collagenase and elastase [21].

To address the specific challenges of diabetic wounds, we developed a glucose/ROS dual-responsive hydrogel (HA-phenylboronic acid (PBA)/polyvinyl alcohol (PVA)/MF, HPM), composed of HA-PBA and PVA. MF was incorporated into the hydrogel *via* dynamic boronate ester bonds. Under high-glucose and high-ROS conditions, glucose competitively binds to boronic acid, and ROS-induced oxidation cleaves the bonds, thereby triggering controlled drug release. The HPM hydrogel exhibits excellent self-healing capability, injectability, and adaptability to wound surfaces, enabling real-time conformation to the dynamically changing wound environment. *In vitro* studies confirmed its favorable biocompatibility and demonstrated significant antioxidant, antibacterial, anti-inflammatory, and cell proliferation-enhancing effects. In a diabetic rat model, HPM significantly accelerated wound healing and tissue regeneration by modulating oxidative stress, reducing inflammation, and promoting angiogenesis.

HA-PBA copolymers were successfully synthesized by covalently grafting PBA onto the HA backbone through an amidation reaction, facilitated by 4-(4,6-dimethoxy-1,3,5-triazine-2-yl)-4-methylmorpholinium chloride (DMTMM) as a coupling agent. Nuclear magnetic resonance (NMR) spectral analysis (Fig. S1a in Supporting information) displayed characteristic peaks at $\delta = 7.46$–7.82 ppm, corresponding to the aromatic protons of the PBA phenyl ring. Peaks observed at $\delta = 3.25$–3.85 ppm and 2.84 ppm were attributed to the protons of the HA backbone and methyl groups, respectively. Based on the integration ratio between the aromatic protons (7.46–7.82 ppm) and the HA methyl protons (2.0 ppm), the degree of carboxyl substitution of PBA was calculated to be 36%, confirming the successful synthesis of the HA-PBA copolymer.

Under physiologically neutral conditions (pH 7.4), HPM hydrogels with potential application in diabetic wound healing were successfully prepared. The vial inversion test (Fig. 1a) showed that HP, HPM-1, and HPM-2 hydrogels rapidly underwent gelation, forming stable three-dimensional network structures. Quantitative measurements (Fig. 1b) revealed gelation times of 11.5 ± 1.6 s for HP, 11.25 ± 1.49 s for HPM-1, and 10.38 ± 1.41 s for HPM-2, with no significant differences among the groups ($P > 0.05$). Notably, the incorporation of MF did not impede gelation; instead, it slightly shortened gelation time, suggesting a potential role in promoting the crosslinking process.

Fourier transform infrared spectroscopy (FTIR) spectroscopy (Fig. S1b in Supporting information) further confirmed the successful formation of HPM hydrogels. The identified characteristic absorption peaks included a broad band at 3306 cm^{-1} (O–H/N–H stretching vibrations from HA and PVA hydroxyl groups and MF amino groups), a peak at 2924 cm^{-1} (C–H stretching from the polymer backbone), a strong peak at 1616 cm^{-1} (C=O stretching, amide I band, indicating successful amidation between HA and PBA), a peak at 1373 cm^{-1} (B–O vibrations, indicating boronate ester bond formation), and a peak at 1034 cm^{-1} (C–O stretching, characteristic peak of PVA). The B–O peak at 1373 cm^{-1} confirmed the formation of dynamic boronate ester bonds between the boronic acid groups of HA-PBA and *cis*-diol groups of MF/PVA. Additionally, the amide I band at 1616 cm^{-1} further substantiated the successful amidation reaction between PBA and HA.

All hydrogels, HP, HPM-1, and HPM-2, exhibited good homogeneity (Fig. 1c). HP hydrogel was transparent, while HPM-1 and HPM-2 appeared light yellow-green due to MF incorporation. Scanning electron microscope (SEM) analysis (Fig. 1d and Fig. S2a in Supporting information) demonstrated that all hydrogels possessed uniform porous structures with consistent pore size distribution and interconnected channels in cross-section, indicating that the addition of MF did not significantly alter the hydrogels' morphological features.

Swelling behavior tests (Fig. 1e) revealed excellent water absorption capacities for all hydrogels. Within 2 h, swelling ratios exceeded 1000%, reaching equilibrium at approximately 6 h. HP hydrogel showed the highest equilibrium swelling ratio (1621% ± 82.39%), whereas HPM-2 exhibited a slightly lower swelling ratio (1459% ± 148.2%) due to increased crosslinking density from higher MF content. Statistical analysis confirmed no significant differences in swelling performance among the three hydrogel groups ($P > 0.05$).

Rheological tests demonstrated that all three hydrogels possess excellent mechanical properties. The amplitude sweep results (Figs. S2b–d in Supporting information) showed that the storage modulus (*G*') of each hydrogel was substantially higher than the loss modulus (*G*"), with HPM-1 exhibiting the highest *G*' value (1066 Pa), indicating superior elasticity. Shear rate tests (Figs. S2e–g in Supporting information) confirmed the hydrogels' pronounced shear-thinning behavior, as their viscosity decreased from 491.95 Pa·s to 602.12 Pa·s at a low shear rate (0.1 rad/s) to 27.68–33.9 Pa·s at a high shear rate (100 rad/s). This property imparts both injectability and conformability to wound surfaces. Cyclic strain tests (Figs. S2h–j in Supporting information) further demonstrated that, due to the reversible nature of dynamic boronate ester bonds, the hydrogels could recover 65%–76% of their original modulus within 2 min after mechanical damage, indicating strong self-healing capability.

Self-healing performance tests (Fig. 1f) showed that, owing to the reversible crosslinking of dynamic boronate ester bonds, two separate hydrogel segments could autonomously rejoin within 2 min and withstand tensile stress without rupture after 5 min. This rapid self-repair ability enables the hydrogels to accommodate joint motion stress, providing continuous protection at wound sites. Adhesion assessments (Fig. 1g) indicated that all three hydrogels exhibited excellent tissue adhesion. They adhered firmly to internal organs and articulating surfaces, maintaining stable attachment even after repeated mechanical deformation. Notably, HPM-2 showed the strongest adhesion, attributed to its higher grafting density of phenylboronic acid groups, which enhances interaction with tissue surfaces and strengthens the crosslinked network through MF polyphenol groups. Adaptive performance evaluations (Fig. 1h) revealed that the hydrogels could gradually fill complex voids under gravity, enabling them to conform effectively to irregular wound geometries, particularly beneficial for treating deep, uneven diabetic wounds. Similar to many commercial hydrogel dressings, the HPM hydrogel is designed for convenient application and can readily conform to irregular wound surfaces. Its intrinsic adhesiveness eliminates the need for secondary fixation (*e.g.*, tapes

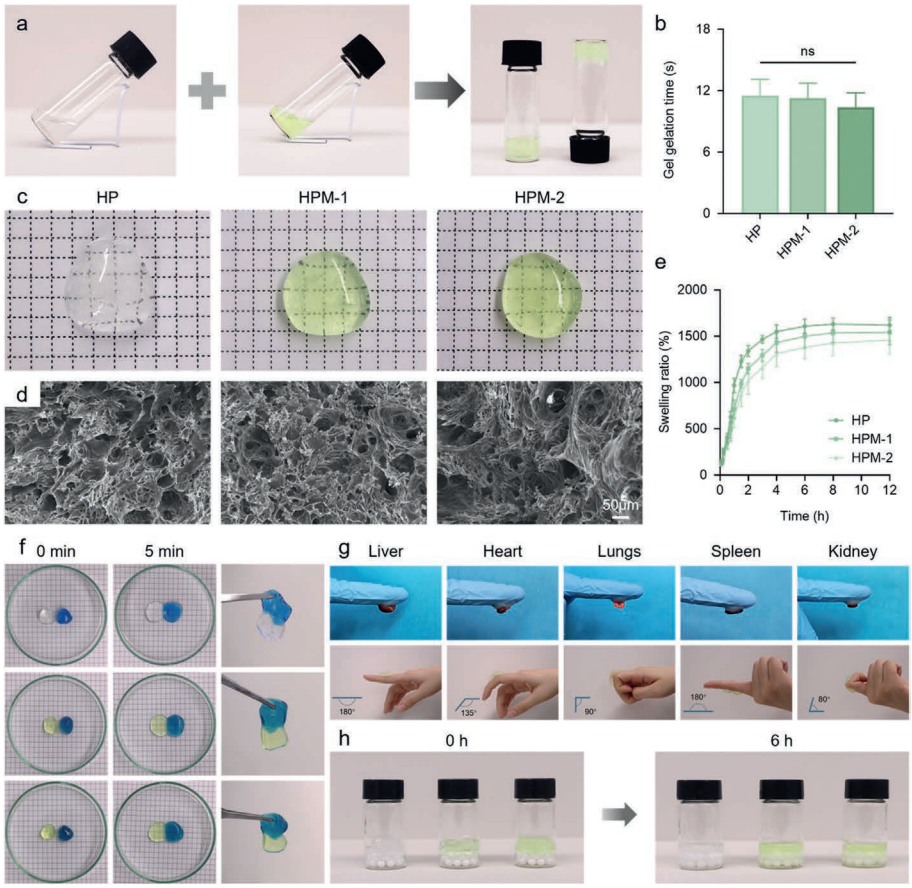


Fig. 1. Preparation and Characterization of Hydrogels. (a) Schematic diagram of gelation transformation of hydrogels. (b) Statistical analysis of the gelation time of hydrogels. ns, not significant. (c) Macroscopic morphology of HP, HPM-1 and HPM-2 hydrogels. (d) SEM images of HP, HPM-1 and HPM-2 hydrogels. (e) Swelling curves of HP, HPM-1 and HPM-2 hydrogels. (f) Self-healing tests of HP, HPM-1 and HPM-2 hydrogels. (g) Adhesion test of HPM-2 hydrogel for animal internal organs and joints. (h) Adaptive testing of HP, HPM-1 and HPM-2 hydrogels. Data are presented as mean ± standard deviation (SD) ($n = 4$). $^{*}P < 0.05$, $^{**}P < 0.01$, $^{***}P < 0.001$.

or films), offering a clear advantage over non-adhesive commercial sheets.

As shown in Fig. S3 (Supporting information), degradation studies (Fig. S3a) demonstrated that HPM-2 hydrogels exhibit dual responsiveness to glucose and ROS. In a simulated diabetic wound environment containing 40 mmol/L glucose and 1 mmol/L H_2O_2, the hydrogel fully degraded within 6 h, at a significantly faster rate than under single-stimulus (glucose or H_2O_2 alone) or PBS control conditions. Drug release experiments (Figs. S3b and c) revealed that HPM-2 hydrogels exhibit environment-responsive drug delivery. In the presence of glucose, phenylboronic acid groups preferentially bind to *cis*-diols, loosening the network and increasing the MF release rate in a glucose concentration-dependent manner. In oxidative conditions, H_2O_2 oxidizes phenylboronic acid groups, irreversibly disrupting the network and further accelerating drug release with rising H_2O_2 concentrations. Notably, the highest drug release rate was observed under combined stimuli (1 mmol/L H_2O_2 + 40 mmol/L glucose). However, elevated H_2O_2 concentrations may cause oxidative degradation of MF molecules, leading to a decline in drug concentration during the later release phase. This graded responsiveness, in which the release rate is directly correlated with the intensity of the pathological stimulus, provides strong evidence that our hydrogel can enable on-demand drug release specifically triggered by the diabetic wound microenvironment.

The MTT assay results (Fig. S3e) demonstrated that NIH 3T3 cell viability remained above 94 % after 24 and 48 h of exposure to hydrogel extracts, compared to the control group ($P > 0.05$), indicating no significant cytotoxicity of the material. Live/dead cell staining (Fig. S3d) further confirmed that the density of live cells (green fluorescence) in the hydrogel group was comparable to that in the control group, with only a few scattered dead cells (red fluorescence). Notably, cell proliferation was observed after 48 h, further supporting the material's excellent cytocompatibility. Additionally, hemolysis tests (Figs. S3f and g) showed that the hemolysis rates for all hydrogel groups were below 1 %, well below the safety threshold [22], confirming that the hydrogel meets the hemocompatibility requirements for biomedical applications.

To definitively assess whether the antioxidative activity of MF arises from a direct radical-scavenging mechanism, we first performed a 1,1-diphenyl-2-picrylhydrazyl (DPPH) assay. This cell-free chemical method is a widely accepted approach for evaluating a compound's direct electron-donating capacity. As shown in Fig. S4, results from the DPPH free radical scavenging assay (Figs. S4a and b) revealed that HPM-1 and HPM-2 hydrogels containing MF exhibited significantly greater scavenging activity (76.85 %–78.28 %, $P < 0.05$) compared to the HP hydrogel (22.5 % ± 0.68 %). These findings provide direct chemical evidence that MF acts as a potent antioxidant by donating hydrogen atoms or electrons to neutralize free radicals. The DCFH-DA assay (Fig. 2a) showed that HPM-2 hydrogel effectively reduced H_2O_2-induced ROS levels to near those of the blank group. Flow cytometry analysis (Figs. S4d and e) further confirmed a dose-dependent ROS scavenging effect of HPM hydrogels. Mechanistic studies (Figs. S4c and f) revealed that HPM hydrogels significantly enhanced superoxide dismutase (SOD) activity ($P < 0.05$) and decreased malondialdehyde (MDA)

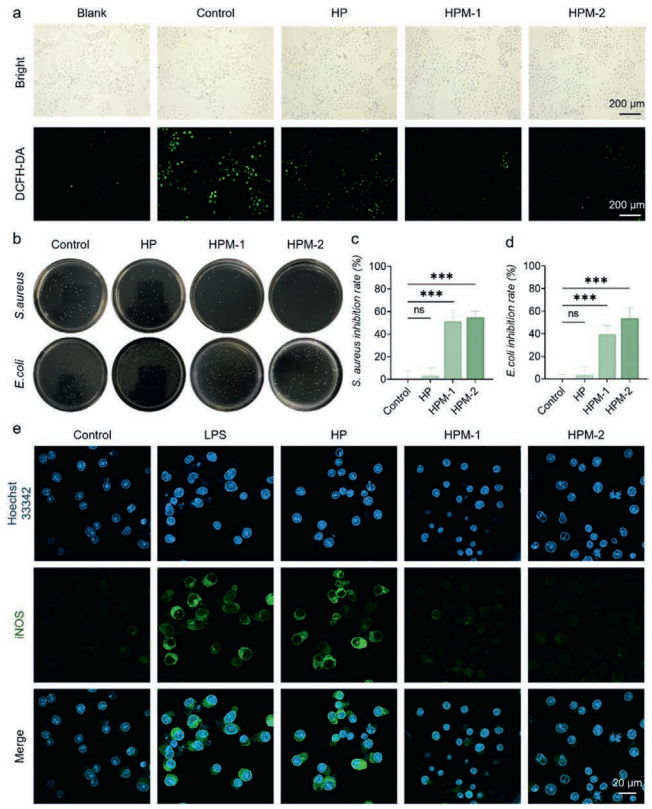


Fig. 2. Evaluation of the biological activity of synthetic hydrogels. (a) DCFH-DA fluorescence staining of NIH 3T3 cells after hydrogel treatment. (b) Colony counts of *S. aureus* and *E. coli* after hydrogel treatment. (c) Statistical analysis of *S. aureus* colony count after hydrogel treatment. (d) Statistical analysis of *E. coli* colony counts after hydrogel treatment. (e) iNOS immunofluorescence images of RAW 264.7 cells treated with hydrogel. Data are presented as mean ± SD ($n = 3$). $^{*}P < 0.05$, $^{**}P < 0.01$, $^{***}P < 0.001$.

levels ($P < 0.05$), indicating that they offer comprehensive antioxidant protection for diabetic wounds by boosting the endogenous antioxidant defense system and inhibiting lipid peroxidation.

As shown in Fig. S5, the agar diffusion assay (Figs. S5a–c) revealed that the HPM-1 and HPM-2 hydrogels formed distinct zones of inhibition against both bacterial strains. The colony counting assay (Figs. 2b–d) further demonstrated that the MF-loaded HPM hydrogels significantly decreased bacterial viability ($P < 0.05$), whereas no significant difference was observed between the HP hydrogel and control groups. The live/dead staining results (Figs. S5d and e) were consistent with the above findings, demonstrating a marked increase in the proportion of dead (red fluorescent) bacteria following HPM treatment. These results suggest that the incorporation of MF imparts the hydrogels with potent and broad-spectrum antibacterial properties.

Reverse transcription quantitative polymerase chain reaction (RT-qPCR) analysis (Figs. S5f–i) revealed that lipopolysaccharide (LPS) stimulation significantly increased the mRNA expression of pro-inflammatory markers, including tumor necrosis factor-alpha (TNF-α), interleukin-1beta (IL-1β), IL-6, and inducible nitric oxide synthase (iNOS), in RAW 264.7 cells. Treatment with HPM hydrogels inhibited the expression of these inflammatory factors in a dose-dependent manner, with HPM-2 demonstrating the most significant suppressive effect ($P < 0.05$). Immunofluorescence staining (Fig. 2e, Figs. S5j and k) further validated that HPM hydrogels effectively reduced iNOS protein levels, with the inhibitory effect intensifying as the MF concentration increased. These findings suggest that the hydrogels may alleviate the inflammatory microenvironment by modulating macrophage polarization.

The scratch assay (Figs. S6a, c and d in Supporting information) demonstrated that HPM hydrogels significantly enhanced the migratory capacity of human umbilical vein endothelial cells (HUVECs). After 24 h of incubation, the wound closure rate in the HPM-2 group (56.33 % ± 1.66 %) was significantly higher than that in the control group (41.11 % ± 3.63 %, $P < 0.05$). At 48 h, the closure rates further increased to 86.74 % ± 1.26 % and 82.16 % ± 2.04 % in the HPM-2 and HPM-1 groups, respectively, both substantially surpassing that of the control group (64.73 % ± 1.87 %). These results indicate that MF incorporation enhances the hydrogel's capacity to promote cell migration.

The *in vitro* angiogenesis assay (Figs. S6b, e and f in Supporting information) showed that HPM hydrogels markedly improved the tube formation ability of HUVECs. After 6 h of incubation, the HPM groups formed more complex tubular networks, characterized by significantly increased tube length and meshes density compared to the control group ($P < 0.05$). These enhancements were dependent on MF concentration, with HPM-2 exhibiting the most pronounced effect, confirming its potent pro-angiogenic activity, which may facilitate diabetic wound healing by accelerating neovascularization.

Topical application of the hydrogel as a wound dressing was selected to closely replicate clinical practices for managing chronic and acute wounds. This approach ensures continuous and direct contact between the hydrogel and the wound bed, which is essential for localized drug delivery and for maintaining a moist, protective healing environment. The dosing regimen was thoughtfully designed based on the distinct biological phases of wound healing. During the initial inflammatory phase, frequent dressing changes help remove excess exudate and debris, thereby reducing bacterial load and minimizing the risk of infection. As the wound progresses into the proliferative phase, less frequent changes are preferred to avoid disturbing the newly formed granulation tissue and epithelium, both critical for efficient healing and for reducing patient discomfort in clinical settings. Animal experiments were approved by the Institutional Animal Care and Use Committee of Sun Yat-sen University (No. SYSU-IACUC-2024–000,223). As illustrated in Figs. 3a and b, the HPM hydrogel treatment group exhibited a marked enhancement in wound closure, with the HPM-2 group demonstrating the most pronounced effect. Quantitative analysis (Fig. 3c) revealed that, by day 14 post-treatment, the wound closure rate in the HPM-2 group reached 94.92 % ± 1.64 %, which was significantly higher than that of the control group (79.86 % ± 6.95 %, $P < 0.05$). These findings confirm that the incorporation of MF markedly enhances the hydrogel's capacity to facilitate wound healing in diabetic models.

As shown in Fig. S7 (Supporting information), the subcutaneous implantation experiment (Fig. S7a) demonstrated that the hydrogel integrated effectively with host tissue, inducing only mild neutrophil infiltration and localized vasodilation, without any evident signs of rejection or fibrosis. Histopathological analysis (Fig. S7b) confirmed that the major organs of the experimental animals, including the heart, liver, spleen, lungs, and kidneys, maintained normal tissue architecture following hydrogel implantation, with no signs of inflammation, necrosis, or other pathological changes. Blood biochemical analyses (Figs. S7c–f) revealed that key serum indicators, including aspartate aminotransferase (AST), alanine aminotransferase (ALT), blood urea nitrogen (BUN), and creatinine (Cr), remained within normal ranges across all hydrogel-treated groups. Notably, the HPM-2 group exhibited a significantly reduced serum Cr level ($P < 0.05$), suggesting a potential renoprotective effect.

Hematoxylin and eosin (H&E) staining (Fig. 4a) revealed that the HPM hydrogel-treated group exhibited a substantially attenuated inflammatory response by day 3, with the HPM-2 group showing minimal inflammatory cell infiltration and early colla-

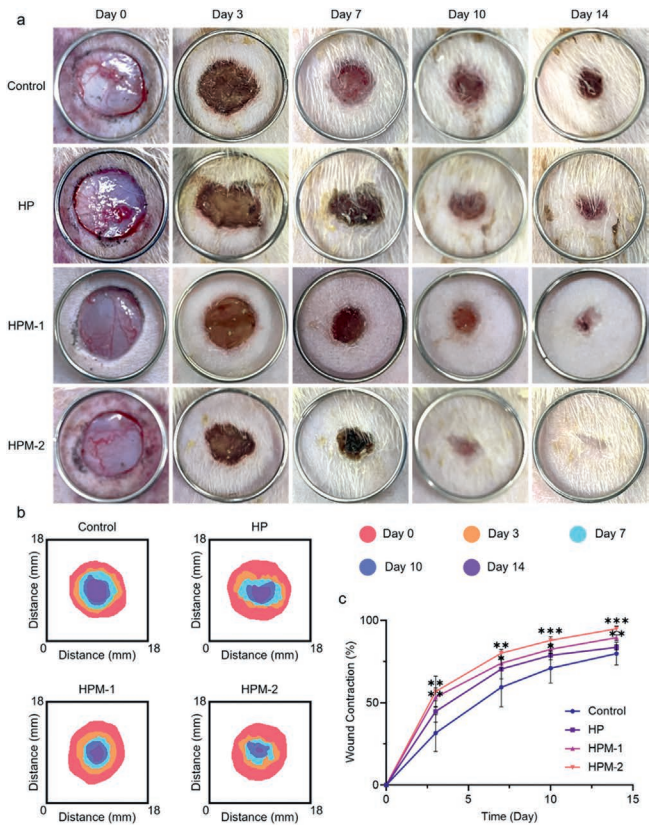


Fig. 3. Wound repair results of diabetic rats. (a) Representative images of wound repair in diabetic rats. (b) Representative superimposed schematic diagram of wound repair in diabetic rats. (c) Statistical analysis of wound repair in diabetic rats. Data are presented as mean ± SD ($n = 4$). $^{*}P < 0.05$, $^{**}P < 0.01$, $^{***}P < 0.001$.

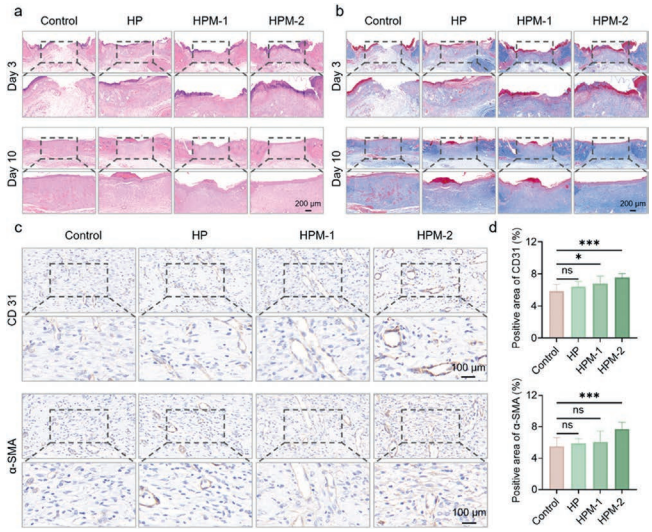


Fig. 4. Immunostaining results of H&E, Masson, CD 31 and α-SMA in wound tissue. (a) Representative images of H&E staining of wound tissues in diabetic rats. (b) Representative images of Masson staining of wound tissues in diabetic rats. (c) Representative images of CD 31 and α-SMA immunofluorescence staining in wound tissue sections of diabetic rats. (d) Statistical analysis of CD 31 and α-SMA immunofluorescence staining in wound tissue sections of diabetic rats. Data are presented as mean ± SD ($n = 3$). $^{*}P < 0.05$, $^{**}P < 0.01$, $^{***}P < 0.001$.

gen fiber formation. By day 10, the HPM-2 group demonstrated superior tissue repair, characterized by continuous epidermal regeneration and significantly thickened granulation tissue. Masson's trichrome staining (Fig. 4b) further confirmed that the HPM-2 group exhibited denser and more organized collagen fiber deposition, forming a tissue architecture closely resembling normal skin.

Immunofluorescence staining results indicated that during the critical inflammatory phase of wound healing, the MF-containing HPM hydrogel-treated group exhibited significant anti-inflammatory effects, with substantially reduced expression levels of pro-inflammatory cytokines such as TNF-α and IL-6 compared to the control group. Moreover, this inhibition showed a concentration-dependent relationship with MF content (Fig. S8a in Supporting information).

Immunohistochemical staining on day 6 of wound healing (Figs. 4c and d) demonstrated that the HPM hydrogel treatment group exhibited a significant pro-regenerative effect. CD31-positive staining areas were markedly increased, indicating active vascular endothelial cell proliferation and enhanced neovascularization. Concurrently, α-SMA expression was significantly upregulated, suggesting increased differentiation of myofibroblasts and an accelerated tissue remodeling process. This promotive effect exhibited a clear dependence on MF concentration, with the HPM-2 group displaying the most pronounced outcome.

Sirius Red staining (Fig. S8b in Supporting information) further confirmed a substantial enhancement of collagen deposition in the HPM hydrogel-treated group. Compared to the control, the HPM-2 group showed a notable increase in collagen fiber density, with significantly elevated proportions of both type I and type III collagen.

This study successfully developed a novel dynamic hydrogel drug delivery system based on HA, PBA and MF. This material exhibits excellent physicochemical properties and dual-responsive release characteristics to both glucose and ROS. The constituent materials are commercially available or naturally derived, with relatively low costs. The synthesis process is simple and straightforward, conducted at room temperature without the need for specialized conditions, thus avoiding high costs and complex synthesis steps. Notably, the strong adhesiveness to moist tissue surfaces ensures that the hydrogel remains securely in place after application, protecting the wound from external contaminants. Additionally, the hydrogel's integrity in experimental settings indicates that it can be removed intact without leaving debris, thereby minimizing trauma during dressing changes. This provides an innovative solution for the treatment of diabetic wounds.

Although not directly confirmed in this study, the observed therapeutic efficacy can be plausibly explained by well-established molecular mechanisms. The strong antioxidant activity of MF likely activates the Nrf2 signaling pathway, a central regulator of cellular antioxidant responses, which mitigates oxidative stress and consequently suppresses the nuclear factor-κB (NF-κB)-mediated pro-inflammatory cascade. This attenuation of chronic inflammation may, in turn, facilitate the transition from the inflammatory to the proliferative phase of wound healing, thereby fostering a microenvironment conducive to fibroblast migration, collagen deposition (potentially *via* transforming growth factor-β/Smad signaling), angiogenesis, and re-epithelialization. Thus, we propose that the hydrogel promotes tissue regeneration by disrupting the vicious cycle of oxidative stress and chronic inflammation, thereby establishing a pro-regenerative microenvironment.

It is important to note that this study employed a conventional induced diabetic model lacking major vascular complications, representing a specific but common patient subgroup. The hydrogel's performance may vary in wounds with different underlying pathologies, such as severe ischemia or critical colonization. Nevertheless, due to its modular design, we anticipate that the hy-

drogel's properties, such as its antioxidant and immunomodulatory functions, can be tailored to meet the specific needs of various wound types. For instance, incorporating pro-angiogenic or antimicrobial agents could enhance its efficacy in ischemic or infected wounds, respectively. This represents a promising direction for future research.

CRediT authorship contribution statement

Lele Meng: Writing – original draft, Visualization, Validation, Methodology, Investigation, Formal analysis. **Ruhe Zhang:** Writing – review & editing, Methodology, Formal analysis, Conceptualization. **Liying Wang:** Writing – review & editing, Supervision, Resources, Data curation, Conceptualization. **Yuanzheng Wang:** Writing – review & editing, Funding acquisition. **Bo Li:** Writing – review & editing, Funding acquisition. **Long Chen:** Supervision, Resources, Funding acquisition, Data curation, Conceptualization.

Declaration of competing interest

The authors declare that they have no known competing financial interests or personal relationships that could have appeared to influence the work reported in this paper.

Acknowledgments

This work was supported by the National Natural Science Foundation of China (Nos. 82302772 and 82160419), Guizhou Basic Research Project (Nos. ZK [2023] General 201 and ZK [2022] General 259), Medical Research Joint Fund project of Guizhou Province (No. 2024GZYXKYJJXM0041) and Doctoral Fund of Guizhou Provincial People's Hospital (No. GZSYBS[2019]01).

Supplementary materials

Supplementary material associated with this article can be found, in the online version, at doi:10.1016/j.cclet.2025.111981.

References

[1] Q. Yang, D. Fang, J. Chen, et al., Theranostics 13 (2023) 3655–3674.
[2] L. He, S. Xing, W. Zhang, et al., Carbohydr. Polym. 354 (2025) 123316.
[3] Y. Liao, Z. Zhang, W. Hu, et al., Biomaterials 318 (2025) 123182.
[4] Z. Liu, H. Li, Y. Huang, et al., Chem. Eng. J. 506 (2025) 159813.
[5] T. Wang, Y. Zheng, J. Zhang, Z. Wu, Heliyon 10 (2024) e37477.
[6] P. Kowalczyk, S. Krych, K. Kramkowski, A. Jęczmyk, T. Hrapkowicz, Int. J. Mol. Sci. 25 (2024) 12467.
[7] J. Wang, Z. Gao, H. Liang, et al., Chin. Chem. Lett. 36 (2025) 110569.
[8] Y. Yang, S. Huang, Q. Ma, et al., Regen. Biomater. 11 (2024) rbae062.
[9] F. Dai, J. Zhang, F. Chen, et al., Adv. Sci. 11 (2024) 2408783.
[10] J. Wang, X. Ge, Y. Xiang, et al., Chin. Chem. Lett. 36 (2025) 109819.
[11] J. Wang, Y. Yang, H. Xu, et al., Nano-Micro Lett. 17 (2025) 171.
[12] L. Qi, C. Zhang, B. Wang, J. Yin, S. Yan, Macromol. Biosci. 22 (2022) 2100475.
[13] Z.P. Zhou, X. Wei, M. Yan, et al., Chin. Chem. Lett. 36 (2025) 111400.
[14] J. Cui, J. Shi, Y. Liu, et al., Chem. Eng. J. 507 (2025) 160379.
[15] S. Zhu, Q. Dai, L. Yao, et al., Compos. Part B: Eng. 231 (2022) 109569.
[16] S. Yang, Q. Zhou, B. Zhang, et al., Nat. Prod. Bioprospect. 10 (2020) 187–200.
[17] M. Baghel, I. Baghel, P. Kumari, et al., Appl. Biochem. Biotechnol. 196 (2024) 7429–7463.
[18] A. Athipornchai, P. Pabunrueang, T. Trakulsujaritchok, Food Hydrocoll. 147 (2024) 109394.
[19] M. Pleguezuelos-Villa, A. Nácher, M.J. Hernández, et al., Int. J. Pharm. 564 (2019) 299–307.
[20] E.V. Fomenko, Y. Chi, BioFactors 42 (2016) 492–503.
[21] M. Sguizzato, F. Ferrara, S.S. Hallan, et al., Antioxidants 10 (2021) 768.
[22] Y. Wu, Y. Wang, L. Long, et al., J. Control. Release 341 (2022) 147–165.